Engineering Structures 236 (2021) 112126

Contents lists available at ScienceDirect

Engineering Structures

journal homepage: www.elsevier.com/locate/engstruct

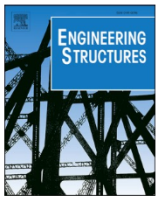

Long-term extreme buffeting response of cable-supported bridges with uncertain turbulence parameters

Tor M. Lystad [a,b,*], Aksel Fenerci [b], Ole Øiseth [b]

[a] Bridge Department, Norconsult AS, Sandvika, Norway
[b] Department of Structural Engineering, Norwegian University of Science and Technology, Trondheim, Norway

ARTICLE INFO

Keywords:
Long-span bridge
Extreme response
Long-term response
Turbulence variability

ABSTRACT

Although the full long-term method (FLM) is recognized as the appropriate way to identify the design stresses of marine structures subjected to stochastic environmental loading, the FLM has not yet been adopted for the design of wind excited long-span bridges. The results presented in this study show that the current design practice, through short-term extreme response analyses with deterministic turbulence parameters, may significantly underestimate the long-term design stresses of long-span bridges. Both the variability of the turbulence parameters and the uncertainty in the short-term extreme response are found to be important when estimating the design stresses. In addition, the long-term extreme acceleration responses have been compared with the acceleration responses measured in full scale at the Hardanger Bridge, showing considerable improvements to the current design practice.

1. Introduction

Several full-scale measurement campaigns around the world have identified large variability in the measured dynamic response of long-span bridges subjected to wind loading [1–7]. By accounting for the uncertainty in the turbulence field, it was found in [8,9] that the variability in the measured acceleration response of the Hardanger Bridge could be predicted. They also showed that the design guidelines strongly underpredicted the largest root-mean-square acceleration responses measured in full scale at the Hardanger Bridge. The observations from these studies indicate a need to revisit the design practice for long-span bridges, especially as bridges become increasingly longer and more sensitive to dynamic wind loading [10].

The characteristic load effect used in structural design calculations is defined by a yearly exceedance probability, p. This probability can be expressed through a statistical return period in years, $p = 1/R_{yr}$. A common simplification in design calculations for linear systems is to define the return period of the load effect equal to the return period of the load. This approach will, in general, not be correct for a cable-supported bridge subjected to turbulent wind loading since the load effect will be a stochastic process. However, in current bridge engineering practice, this simplification is widely used, and the characteristic load effect is calculated as the expected extreme response from a short-term storm defined by a mean wind velocity with a return period, R_{yr}, and its corresponding deterministic turbulence parameters. This approach introduces two important assumptions: 1) the variability of the turbulence parameters can be neglected or treated in a simplified manner, and 2) the uncertainty of the short-term extreme peak response can be treated deterministically by its expected value.

In recent years, some studies have investigated the effect of these assumptions. Lystad et al. [8] investigated the effect of uncertain turbulence parameters on the buffeting response of the Hardanger Bridge using the environmental contour method (ECM), identifying considerable effects on the prediction of the largest bridge response. Xu et al. [11] found that due to the uncertainty of the short-term response, the long-term extreme response would significantly exceed the expected value of the short-term extreme buffeting response of a long-span suspension bridge. This effect is well-known in the field of marine engineering [12,13], and standards for the design of offshore structures already recommend accounting for such effects [14]. These studies indicate that the abovementioned simplifications may introduce significant inaccuracies in the current design practice.

Long-term extreme value methodology is recognized as the most accurate way to estimate the extreme load effects from stochastic environmental excitation of marine structures [15]. In such calculations, the R_{yr} return period load effect is calculated directly, accounting for the

* Corresponding author at: Bridge Department, Norconsult AS, Sandvika, Norway.
E-mail address: tor.m.lystad@ntnu.no (T.M. Lystad).

https://doi.org/10.1016/j.engstruct.2021.112126
Received 23 November 2020; Received in revised form 18 February 2021; Accepted 23 February 2021
Available online 15 March 2021

uncertainty of the structural response. The important parameters defining the load process are treated as stochastic variables and described by a joint probability distribution.

Several formulations of the full long-term method (FLM) exist [16], and they all need to integrate the short-term response statistics over all relevant environmental combinations, making them very computationally demanding. The long-term extreme value problem can also be solved by simplified reliability methods such as the inverse first-order reliability method (IFORM) [17,18] and the environmental contour method (ECM) [19]. These methods are attractive because they are relatively efficient from a computational perspective. The IFORM can be used to estimate the R_{yr} return period long-term extreme response directly, where the short-term extreme response is included as a random variable. The ECM is an inverse reliability method that can be used to identify R_{yr} return period short-term load situations based on the joint probability of several environmental variables. The environmental contour method separates the variability of the environmental parameters and the uncertainty of the short-term extreme response itself. Therefore, to estimate the long-term extreme load effect, the omission of this variability needs to be corrected.

Probabilistic frameworks in wind engineering have been investigated in the literature [20–29]. These frameworks focus mostly on uncertainties in the load and the structural properties with methods to estimate the reliability of the structure. With the FLM, the probability distribution of the extreme response of a system subjected to stochastic environmental loads is calculated. This process is valuable since the R_{yr} return period load effect can be drawn directly from this distribution to be used in ordinary design calculations, but it can also provide valuable information for possible structural reliability considerations.

In this paper, long-term extreme value methodology is used to investigate the extreme design stresses in the Hardanger Bridge girder due to turbulent wind loading. In Section 2, the theoretical basis is outlined, and in Section 3, the buffeting analyses are described. In Section 4, long-term extreme value predictions are presented for the design stresses of the Hardanger Bridge girder, showing significant effects from extreme value- and turbulence uncertainty on the extreme stresses. The FLM, IFORM and ECM are all used to estimate the long-term extreme response. Furthermore, in Section 5, long-term extreme acceleration response predictions are compared with full-scale measurements, showing considerable improvements to the current design practice.

2. Extreme response calculation methods

For the ultimate limit state design of structures subjected to stochastic wind loads, three approaches can be used to estimate the design load effects:

- The short-term design wind speed approach
- The short-term environmental contour method
- The long-term design approach.

In a short-term extreme value calculation, stationary and ergodic extreme storm conditions with a statistical return period R_{yr} are defined by a set of environmental variables given by the vector $\mathbf{w}$. In the short-term design wind speed approach, the environmental variables are defined by the event of a mean wind velocity with a return period R_{yr}, and the corresponding turbulence parameters are chosen deterministically. In the short-term environmental contour method, the extreme storm condition is defined by the environmental contour method, accounting for the variability in the turbulence parameters as well as the mean wind velocity.

When considering a short-term stochastic response time series from the extreme storm condition defined by $\mathbf{w}$, the largest response during that time window is the short-term extreme response, $\widetilde{R}|\boldsymbol{W}$. However, for another stochastic response realization of the same environmental load definition, $\mathbf{w}$, the extreme peak might be different. Thus, the short-term extreme peak response is uncertain. In current design practice for cable-supported bridges, the expected value of this uncertain peak is used to define the design load effects, $E[\widetilde{R}|\boldsymbol{W}]$, based on the short-term design wind speed approach.

In a long-term design approach, a long-term time window is defined by a sequence of short-term time series. Then, the cumulative probability density function of the long-term extreme response is established, $F_R(r,\ 0 \le t < T)$. This function is calculated based on the response statistics of each short-term condition, weighted by the probability of the environmental parameters, $f_{\boldsymbol{W}}(\boldsymbol{w})$. In this way, the extreme response with a statistical return period can be calculated directly from $F_R(r,\ 0 \le t < T) = 1\text{-}p = 1\text{–}1/R_{yr}$,

The methodology presented in this paper relies on the assumption of stationarity within each short-term event. Wind loads are often separated into synoptic and non-synoptic winds [30], and non-synoptic winds can dominate the extreme responses in some areas of the world. Non-synoptic effects can be an important aspect when considering extreme buffeting response [31], and proper investigations needs to be carried out where these events are important. The methodology presented herein focus on the extreme response due to synoptic winds, where the stationarity assumption is reasonable. The strong winds in Norway, and at the Hardanger Bridge site, is dominated by synoptic winds and extratropical cyclones [32] and is a suitable case for investigation of the proposed methodology.

2.1. Short-term extreme response

If the zero-mean response process can be assumed to be Gaussian, ergodic and stationary within a short-term period, $\widetilde{T}$, the short-term extreme peak distribution of that process can be completely defined by the mean upcrossing rate of a threshold, $\widetilde{r}$ [15]. The mean $\widetilde{r}$-upcrossing rate can be defined as:

$$v^+(\widetilde{r}|\boldsymbol{w}) = v^+(0)exp\left\{-\frac{\widetilde{r}^2}{2m_0(\boldsymbol{w})}\right\} \tag{1}$$

where

$$v^+(0) = \frac{1}{2\pi}\sqrt{\frac{m_2(\boldsymbol{w})}{m_0(\boldsymbol{w})}} \tag{2}$$

and $\mathbf{w}$ is the vector containing the environmental variables, $v^+(0)$ is the zero-upcrossing rate and m_i is the i^{th} moment of the response spectrum, $\boldsymbol{S}_{\widetilde{R}|\boldsymbol{W}}(\omega|\boldsymbol{w})$:

$$m_i(\boldsymbol{w}) = \int_0^\infty \omega^i \boldsymbol{S}_{\widetilde{R}|\boldsymbol{W}}(\omega|\boldsymbol{w})d\omega \tag{3}$$

and ω is the angular frequency. Then, the short-term extreme value cumulative density function (CDF) can be defined as follows by introducing the assumption of independent peaks for reasonably large values of $\widetilde{r}$:

$$\begin{aligned} F_{\widetilde{R}|\boldsymbol{W}}(\widetilde{r}|\boldsymbol{w}) &= exp\left\{-v^+(\widetilde{r}|\boldsymbol{w})\widetilde{T}\right\} \\ &= exp\left\{-\frac{\widetilde{T}}{2\pi}\sqrt{\frac{m_2(\boldsymbol{w})}{m_0(\boldsymbol{w})}}exp\left\{-\frac{\widetilde{r}^2}{2m_0(\boldsymbol{w})}\right\}\right\} \end{aligned} \tag{4}$$

The expected value of the short-term extreme peak response can be estimated as follows, given that $ln(v^+(0)\widetilde{T})$ is sufficiently large:

$$E[\widetilde{R}] = k_p\sqrt{m_0(\boldsymbol{w})} \tag{5}$$

where

$$k_p \approx \left\{ \sqrt{2ln(\nu^+(0)\widetilde{T})} + \frac{\gamma}{\sqrt{2ln(\nu^+(0)\widetilde{T})}} \right\} \tag{6}$$

and $\gamma \approx 0.5772$ is the Euler constant, $E[\cdot]$ is the expectation operator and k_p is the short-term peak factor.

2.2. The full long-term method (FLM)

The FLM is relatively simple to use but very computationally demanding since, in principle, the short-term response statistics needs to be calculated and integrated over all possible combinations of the environmental variables, weighted by their probability of occurrence.

Different formulations of the full-long-term method can be found in the literature, but under the appropriate assumptions, they are mathematically equivalent [16].

2.2.1. Formulation based on the upcrossing rate of the short-term response

Naess [33] proposed a formulation that calculates the full long-term extreme value CDF based on the $\widetilde{r}$-upcrossing rate of each short-term process. In the long-term period, T, the response process can no longer be considered a stationary process, so Eq. (4) is generalized for a nonstationary process by replacing the short-term upcrossing rate with its mean value over the long-term period:

$$F_R(r) = exp\left\{ -T\frac{1}{T}\int_0^T \nu^+(r,t)dt \right\} \tag{7}$$

By describing the long-term period as a sequence of stationary short-term periods, the following formulation is reached:

$$F_R(r) = exp\left\{ -T\int_{\mathbf{W}} \nu^+(\widetilde{r}|\boldsymbol{w}) f_{\mathbf{W}}(\boldsymbol{w})d\boldsymbol{w} \right\} \tag{8}$$

where $f_{\mathbf{W}}(\mathbf{w})$ is the joint PDF of the environmental parameters defined in the vector $\mathbf{w}$, $T = N_{st}\widetilde{T}$is the long-term period, and N_{st} is the number of short-term conditions. This formulation is the full long-term formulation with the least limiting assumptions [16], relying only on the ergodicity assumption and that the high-level upcrossings follow a Poisson distribution and will be used in the full long-term calculations in this paper.

2.2.2. Formulations based on all short-term extreme values

In a full long-term calculation, the long-term extreme response CDF is calculated based on the response statistics of each short-term condition. Borgman [34] presented an expression for the long-term extreme value CDF based on the short-term extreme values:

$$F_R(r) = exp\left\{ \int_{\mathbf{W}} ln\left\{ F_{\underset{\sim}{R}|\mathbf{W}}(\widetilde{r}|\boldsymbol{w}) \right\} f_{\mathbf{W}}(\boldsymbol{w})d\boldsymbol{w} \right\} \tag{9}$$

This formulation is valid under the assumption of statistically independent short-term extreme values. The formulation proposed by Borgman [34] is based on ergodic averaging. This is often referred to as the exact formulation of the full long-term extreme value CDF, but it should be noted that it is exact only under the many assumptions previously listed. An approximate formulation of this problem exists as well. This formulation is based on the population mean and not the ergodic average, hence the approximation. The formulation reads:

$$\overline{F}_R(r) = \int_{\mathbf{W}} F_{\underset{\sim}{R}|\mathbf{W}}(\widetilde{r}|\boldsymbol{w}) f_{\mathbf{W}}(\boldsymbol{w})d\boldsymbol{w} \tag{10}$$

This formulation is often a good approximation, although it is strictly unconservative as shown by Jensen's inequality theorem, stating that the expected value of a function is greater than or equal to the expected value of the function after a concave transformation. In Eq. (9), the natural logarithm is a concave function and the following will apply [35]:

$$F_R(r) \leqslant \overline{F}_R(r) \tag{11}$$

and in effect, the R_{yr} return period response quantity estimated by the approximate formulation will be less than or equal to the exact formulation.

2.3. Reliability theory-based calculation methods

2.3.1. Expressing the approximate full long-term formulation as a reliability problem

The approximate formulation for the full long-term extreme value CDF shown in Eq. (10) can be reformulated as a reliability problem. An interesting effect from this reformulation is that it can be solved in an approximate manner using known structural reliability theory such as the first-order reliability method (FORM).

The reliability problem can be written as [36]:

$$p_f = \int_{G(\boldsymbol{x})\leqslant 0} f_{\mathbf{X}}(\boldsymbol{x})d\boldsymbol{x} \tag{12}$$

where p_f is the failure probability, $\mathbf{X}$ is a vector of random variables described by the joint probability density function (PDF) $f_{\mathbf{X}}(\mathbf{x})$, and $G(\mathbf{x})$ is the limit state function in the real space. In the reliability problem, $\mathbf{X}$ contains random variables describing the uncertain load and the uncertain capacity, and then $G(\mathbf{x}) \leq 0$ defines failure. The approximate formulation of the long-term extreme value can be rewritten in a similar form:

$$\overline{F}_R(r) = \int_{\mathbf{W}} F_{\underset{\sim}{R}|\mathbf{W}}(\widetilde{r}|\boldsymbol{w}) f_{\mathbf{W}}(\boldsymbol{w})d\boldsymbol{w} = \int_{\mathbf{W}}\int_{\underset{\sim}{r}\leqslant r} f_{\underset{\sim}{R}|\mathbf{W}}(\widetilde{r}|\boldsymbol{w})d\widetilde{r} f_{\mathbf{W}}(\boldsymbol{w})d\boldsymbol{w} \tag{13}$$

Now, if we define a vector $\boldsymbol{X} = \left[\boldsymbol{W}, \widetilde{R}\right]$, we can construct a joint PDF of the environmental variables and the short-term extreme response as:

$$f_{\mathbf{X}}(\boldsymbol{x}) = f_{\underset{\sim}{R}|\mathbf{W}}(\widetilde{r}|\boldsymbol{w}) f_{\mathbf{W}}(\boldsymbol{w}) \tag{14}$$

and then Eq. (13) is rewritten to the same format as Eq. (12):

$$\overline{F}_R(r) = \int_{\underset{\sim}{r}\leqslant r} f_{\mathbf{X}}(\boldsymbol{x})d\boldsymbol{x} = 1 - \int_{G(\boldsymbol{x})\leqslant 0} f_{\mathbf{X}}(\boldsymbol{x})d\boldsymbol{x} = 1 - p_f \tag{15}$$

where $G(\boldsymbol{x}) = r - \widetilde{r}$.

2.3.2. Expressing the exact full long-term formulation as a reliability problem

Giske et al. [35] proposed a method to formulate the exact full long-term method shown in Eq. (9) as a reliability problem as well, avoiding the strictly unconservative simplification that the approximate formulation introduces. Since $ln\left\{ F_{\underset{\sim}{R}|\mathbf{W}}(\widetilde{r}|\boldsymbol{w}) \right\}$is not a CDF, they rewrote the expression:

$$F_R(r) = exp\left\{ \int_{\mathbf{W}} \left(1 + ln\left\{ F_{\underset{\sim}{R}|\mathbf{W}}(\widetilde{r}|\boldsymbol{w}) \right\} \right) f_{\mathbf{W}}(\boldsymbol{w})d\boldsymbol{w} - 1 \right\} \tag{16}$$

and then introduced a new random variable, Y, so a CDF-like function could be defined as:

$$F_{Y|\mathbf{W}}(y|\boldsymbol{w}) = max\left(1 + ln\left\{ F_{\underset{\sim}{R}|\mathbf{W}}(\widetilde{r}|\boldsymbol{w}) \right\}, 0 \right) \tag{17}$$

Thus, the formulation reads:

$$F_R(r) \approx exp\left\{ \int_{\mathbf{W}} F_{Y|\mathbf{W}}(y|\boldsymbol{w}) f_{\mathbf{W}}(\boldsymbol{w})d\boldsymbol{w} - 1 \right\} \tag{18}$$

Similar to the definition in Eq. (15), the reliability problem becomes:

$$F_R(r) \approx exp\left\{ -\int_{G(\boldsymbol{x})\leqslant 0} f_{\mathbf{X}}(\boldsymbol{x})d\boldsymbol{x} \right\} = exp\{-p_f\} \tag{19}$$

where

$$f_{\boldsymbol{X}}(\boldsymbol{x}) = F_{Y|\boldsymbol{W}}(y|\boldsymbol{w}) f_{\boldsymbol{W}}(\boldsymbol{w}) \tag{20}$$

However, even though this method is based on the exact FLM formulation, the IFORM solution in itself is an approximation.

2.3.3. Solving the long-term extreme value problem using the inverse first-order reliability method (IFORM)

The FORM procedure can be used to calculate the probability of exceedance, p_f, by transforming the random variables in **X** into the standard normal space, **U**, and minimizing the distance to the limit state function:

$$\beta = \text{arg}min|\boldsymbol{u}|; \text{ constrained to } g(\boldsymbol{u}) = 0 \tag{21}$$

where $g(\boldsymbol{u}) = r - \widetilde{r}(\boldsymbol{u}) = 0$ is the limit state function in the standard normal space. β is the reliability index related to the return period as follows:

$$\beta = -\Phi^{-1}(1/[\frac{R_{yr} \times 365.25 \times 24 \times 60}{\widetilde{T}}]) \tag{22}$$

where Φ is the standard normal CDF, R_{yr} is the statistical return period in years, and $\widetilde{T}$ is the short-term duration in minutes.

In the FORM, the limit state function is approximated by a first-order Taylor expansion through the design point identified in the standard normal space [36].

The failure probability is related to the reliability index by the relationship:

$$p_f = \int_{g(\boldsymbol{u}) \leqslant 0} f_U(\boldsymbol{u}) d\boldsymbol{u} = \Phi(-\beta) \tag{23}$$

However, in the inverse FORM procedure, the reliability index is indirectly known through the given return period, and the response, r, is sought. Thus, the solution to the long-term extreme value problem in Eq. is found by maximizing the response under the following constraint:

$$r = \text{arg}max\widetilde{r}(\boldsymbol{u}); \text{ constrained to } |\boldsymbol{u}| = \beta \tag{24}$$

2.3.4. The environmental contour method (ECM)

Winterstein and Haver [19] presented a method based on the IFORM to establish environmental contours for combinations of environmental variables with a combined target statistical return period. The method is also referred to as the IFORM with omission factors since it decouples the variability of the environmental variables from the uncertainty of the structural response itself. In this method, combinations of environmental variables in a standard normal space with a given distance to the origin, namely, the reliability index β, are transformed into the real space based on a joint probability distribution of the environmental variables.

The extreme response is calculated by the short-term method, but it was shown in [19] that the omission factors could be used to inflate the contours to account for the neglected short-term extreme value uncertainty. However, Kleiven and Haver [12] found that the best way to correct for the neglected extreme response uncertainty was by multiplying the expected short-term extreme response by a correction factor or by choosing a higher percentile of the short-term extreme response CDF as the design value. The correction factor is defined as:

$$C_{corr} = \frac{r_{LT}}{\widetilde{r}_{ECM}} \tag{25}$$

where r_{LT} is the long-term extreme response and $\widetilde{r}_{ECM}$ is the expected value of the short-term extreme response found by the ECM. The percentile in the short-term extreme response distribution corresponding to the long-term extreme response is defined by:

$$p_{corr} = F_{\widetilde{R}|\boldsymbol{W}}(r_{LT}) = exp\left\{ -\frac{\widetilde{T}}{2\pi}\sqrt{\frac{m_2(\boldsymbol{w})}{m_0(\boldsymbol{w})}} exp\left(-\frac{r_{LT}^2}{2m_0(\boldsymbol{w})} \right) \right\} \tag{26}$$

where $F_{\widetilde{R}|\boldsymbol{W}}$ is the short-term extreme response CDF defined in Eq. (4).

2.3.5. Finding the design point by the ECM and the IFORM

The design point on the environmental contour can be found by manual iterations and engineering judgment, but it can also be found by numerical optimization [8]. The ECM problem is similar to the IFORM problem, but the number of random variables included is reduced by one in the ECM since the variability of the short-term response itself is excluded. For a system dominated by an environmental load described by two random variables, the environmental contour will be a plane circle in the standard normal space, but the random variables in the IFORM problem will define a sphere in this space. Since the design point solution of both methods needs to have the target distance to the origin, β, the IFORM solution will always fall within the environmental contour when plotted in the two-dimensional space, as illustrated in Fig. 1. Transformation between the real and standard normal space can be performed by different procedures such as the Rosenblatt transformation or by a simple linear transformation [8,37].

The difference in the solution algorithm between the IFORM and the ECM is that with the IFORM, the short-term extreme value $\widetilde{r}(\boldsymbol{u})$ is found directly by transformation of the **u**-vector, but in the ECM, $\widetilde{r}(\boldsymbol{u})$ is treated as a deterministic value given the environmental variables defined by the **u**-vector and is calculated as the short-term expected extreme value defined in Eq. (5).

The iteration algorithm to solve the IFORM problem shown in Eq. (15) and Eq. (19), as proposed by Li and Foschi [17] reads:

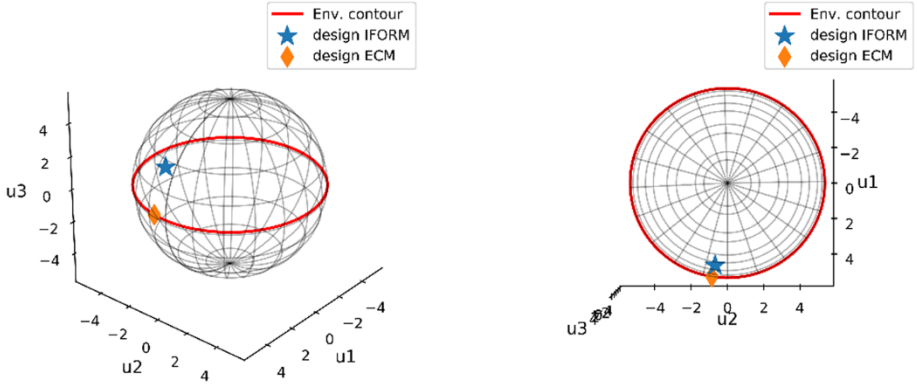

Fig. 1. Illustration of the difference between ECM and IFORM and the effect of the added dimension due to the inclusion of the short-term extreme response uncertainty shown in the standard normal space.

$$\boldsymbol{u}^{k+1} = \beta \frac{\nabla \widetilde{r}_{n+1}(\boldsymbol{u}^k)}{\left|\nabla \widetilde{r}_{n+1}(\boldsymbol{u}^k)\right|} \tag{27}$$

where n is the number of environmental variables and k indicates the iteration. Since the short-term extreme value uncertainty is not included as a variable in the ECM, the expression above reduces to:

$$\boldsymbol{u}^{k+1} = \beta \frac{\nabla \widetilde{r}_{n}(\boldsymbol{u}^k)}{\left|\nabla \widetilde{r}_{n}(\boldsymbol{u}^k)\right|} \tag{28}$$

This simple iteration scheme may fail to converge for some problems, so in the present study, the iteration algorithm defined by Giske et al. [35] was used. This is, in principle, the same algorithm as the one defined by Li and Foschi [17], but a backtracking approach is introduced to avoid diverging iterations. The convergence criterion was defined by the following:

$$\frac{|\boldsymbol{u}^{k+1} - \boldsymbol{u}^k|}{\boldsymbol{u}^{k+1}} < Tolerance \tag{29}$$

A $tolerance = 10^{-3}$ was used in all IFORM and ECM solutions presented in this paper.

3. Buffeting analysis of the Hardanger Bridge

3.1. Probabilistic turbulence model

Fenerci and Øiseth [38] established a site-specific probabilistic model for the Hardanger Bridge (see Fig. 2) wind field representative of the bridge girder elevation based on full-scale measurement data. The model described 6 turbulence parameters as correlated lognormal stochastic variables, conditional on the mean wind velocity and the two dominating wind directions, East and West. The wind directions are channeled by the surrounding terrain, especially for the strong winds [39], so to assume the winds from East and West to be perpendicular to the bridge is a reasonable approximation.

The turbulence spectral model used to define the probabilistic turbulence parameters was a Kaimal-type spectra and a normalized cross-spectra as described in [40,41]:

$$\frac{S_{u,w}f}{\sigma_{u,w}^2} = \frac{A_{u,w}f_z}{(1 + 1.5A_{u,w}f_z)^{5/3}}\ ,\ f_z = \frac{fz}{U}$$
$$C_{u,w} = exp(-K_{u,w}\frac{f\Delta x}{U}) \tag{30}$$

where f is the frequency, z is the height above the ground, U is the mean wind velocity, $\sigma_{u,w}$ are the standard deviations of the along wind- (u) and the vertical (w) turbulence, $A_{u,w}$ are the nondimensional spectral parameters, $K_{u,w}$ are the decay coefficients and Δx is the separation distance along the bridge span. For a quantitative description of the model, the readers are referred to [38].

The mean wind velocity is described using Weibull distributions conditional on the main wind directions, east and west, established in [8,39]. The Weibull PDF model is described in Eq. (31), and the fitted parameters are shown in Table 1.

Table 1
Fitted Weibull distribution parameters [8].

	Weibull distribution	
	λ	k
East	5.1941	1.7946
West	1.4063	0.8616

$$f(u) = \frac{k}{\lambda}\left(\frac{u}{\lambda}\right)^{(k-1)} exp\left\{-\left(\frac{u}{\lambda}\right)^{k}\right\}\ ;\ u \geqslant 0 \tag{31}$$

where k is the shape parameter and λ is the scale parameter.

Based on this model, the vector describing the environmental variables in the long-term analyses will contain one or more of the variables $\boldsymbol{w} = \{U, \sigma_u, \sigma_w, A_u, A_w, K_u, K_w\}$.

3.2. Buffeting analysis

The buffeting analyses are performed in the frequency domain using multimode theory [42–46]. The structural properties are described by a detailed 3D finite element (FE) model in Abaqus [47] shown in Fig. 3, and a structural damping ratio of $\xi = 0.5\%$ was assigned to all vibration modes. The shape and frequency of the most important modes are shown in Table 2. All contributing modes below a cutoff frequency of 1 Hz were included in the analyses. This cutoff frequency is expected to be high enough to describe the stresses well. However, for the acceleration estimates, some contributions from higher frequencies may be excluded by this cutoff frequency. Although this exclusion will result in an underestimation of the acceleration predictions, this choice is made to be consistent with the filtering of the full-scale measurements for comparison reasons.

The girder is modelled with linear Timoshenko beam elements in the FE model. Stiffened steel box girders can be prone to stiffness reductions due to shear-lag effects in the areas of large shear forces, which will not be properly represented with the beam element model used. It is possible to account for this stiffness reduction by modelling the girder with shell elements or by adjusting the beam element formulation [48,49]. For the global buffeting response behavior considered in this paper, the shear forces are modest, and the bending moments are smooth. Therefore, the shear lag effects on the global stiffnesses is expected to be small in the considered application.

The steady-state static coefficients and the aerodynamic derivatives (ADs) for the bridge girder are based on wind tunnel experimental data as described in [50]. The static coefficients are presented in Table 3, and the aerodynamic admittance was neglected. Details on the fitted AD models can be found in [8].

Only the bridge girder and the main cable were subjected to wind loading in the calculations. The static coefficients for the main cables are based on recommendations in Eurocode 1–4 [51] for a painted circular cable and a Reynolds number of approximately 1.5e6, giving a drag coefficient of 1.0. The drag coefficient of the downstream main cable was reduced to 0.7 to account for possible shielding effects. The motion-induced forces on the main cables are described using quasi-steady theory [52].

3.3. Design stresses from stochastic section forces

Most modern suspension bridges today are constructed with a closed box steel girder. These cross-sections are composed of stiffened thin steel plates that can buckle when compressive stresses approach the capacity in the ultimate limit state. Eurocode 3 [53] proposes methods to account for this effect, where parts of the local steel plates under critical pressure are assumed to buckle and be ineffective. These plate parts are removed when the efficient cross-sectional properties are calculated. In addition to local plate buckling, the Eurocode describes methods to account for global buckling of stiffened plate fields. This global buckling is accounted for by reducing the effective thickness of the plates in the pressure zone when the efficient cross-sectional properties are calculated [54]. The Eurocode also states that the effect of plate buckling on the cross-sectional stiffness in an elastic global analysis can be neglected if the effective part of a plate is larger than half the total plate area. This applies for the Hardanger Bridge girder, and the cross-sectional stiffness is based on the full elastic cross section in the buffeting analyses.

Fig. 2. The Hardanger Bridge seen from the northeast (picture by the authors).

Table 2
Frequency and shape of the most important natural modes of the Hardanger Bridge.

Lateral			Vertical			Torsional		
Mode	Freq. [Hz]	Shape	Mode	Freq. [Hz]	Shape	Mode	Freq. [Hz]	Shape
1	0.050	Sym.	3	0.110	Asym.	15	0.359	Sym.
2	0.100	Asym.	4	0.141	Sym.	26	0.523	Asym.
5	0.173	Sym.	6	0.197	Sym.	49	0.783	Sym.
13	0.302	Asym.	7	0.211	Asym.	58	1.006	Asym.
21	0.443	Sym.	12	0.272	Sym.			
34	0.655	Asym.	14	0.329	Asym.			

Table 3
Geometry and steady-state static coefficients used in the buffeting analyses (0-degree angle of attack).

Bridge member	*Width* [m]	*Depth* [m]	C_D	C_L	C_L'	C_M	C_M'
Girder	18.3	3.33	1.050	−0.363	2.220	0.017	0.786
Main cables	0.6	0.6	1.0/ 0.7	0	0	0	0

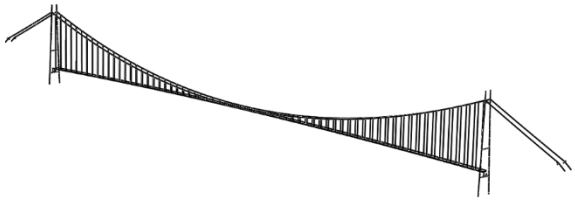

Fig. 3. FEM model of the Hardanger Bridge.

The Eurocode based methodology for the stress calculations are simplified, but suitable for practical applications.

The elastic design stresses for a steel cross-section considering plate buckling can be expressed in a simplified manner according to Eurocode 3 [53] as follows, provided that elastic flexural buckling of the beam is not present:

$$\sigma_{Ed} = \frac{N_x}{A_{eff}} + \frac{M_y + N_x e_z}{W_{eff,y}} + \frac{M_z + N_x e_y}{W_{eff,z}} \tag{32}$$

where A_{eff} is the effective area for pure compressive axial force (N_x), $W_{eff,y}$ is the effective section modulus for pure weak-axis bending (M_y) and $W_{eff,z}$ is the effective section modulus for pure strong-axis bending (M_z). The eccentricities e_y and e_z describe the shift of the neutral axes under pure compression of the cross-section. To estimate the stresses from a buffeting analysis, the contribution from each section force response process can be added according to Eq. (32). In a time-domain analysis, the stress process can be calculated directly based on the section force combination in each time step. In a frequency-domain analysis, the extreme response statistics can be performed directly on the stress process by utilizing the information available from the section force response cross-spectral density matrix.

Each section force process will contribute to the stresses at a considered point. To obtain the total stresses, the variance of a sum of correlated Gaussian processes is needed. From Eq. (32) we get:

$$\begin{aligned} m_{i,\sigma_{Ed}} &= m_{i,Z_1Z_1} + m_{i,Z_2Z_2} + m_{i,Z_3Z_3} + 2m_{i,Z_1Z_2} + 2m_{i,Z_1Z_3} + 2m_{i,Z_2Z_3} \\ m_{i,\sigma_{Ed}} &= a^2 m_{i,N_xN_x} + b^2 m_{i,M_yM_y} + c^2 m_{i,M_zM_z} + 2abm_{i,N_xM_y} + 2acm_{i,N_xM_z} + 2bcm_{i,M_yM_z} \end{aligned} \tag{33}$$

where

$$\begin{aligned} Z_1(t) &= \left(\frac{1}{A_{eff}} + \frac{e_z}{W_{eff,y}} + \frac{e_y}{W_{eff,z}}\right) N_x(t) = aN_x(t) \\ Z_2(t) &= \frac{1}{W_{eff,y}} M_y(t) = bM_y(t) \\ Z_3(t) &= \frac{1}{W_{eff,z}} M_z(t) = cM_z(t) \end{aligned} \tag{34}$$

From the frequency-domain buffeting analysis, the full response

spectral density matrix is established as:

$$\boldsymbol{S}_r(\omega) = \begin{bmatrix} S_{N_x N_x}(\omega) & S_{N_x M_y}(\omega) & S_{N_x M_z}(\omega) \\ S_{M_y N_x}(\omega) & S_{M_y M_y}(\omega) & S_{M_y M_z}(\omega) \\ S_{M_z N_x}(\omega) & S_{M_z M_y}(\omega) & S_{M_z M_z}(\omega) \end{bmatrix} \tag{35}$$

Then, the i^{th} moment of the response cross spectral density can be calculated as:

$$m_{i,kl} = \int_0^\infty \omega^i S_{kl}(\omega) d\omega \tag{36}$$

where $i = 0$ defines the covariance of the response, and $i = 2$ defines response rate. In this way, the 0th and 2nd moments of the stress response spectrum needed to define Eq. (1) can be estimated.

The Hardanger Bridge girder cross-section is shown in Fig. 4. The top plate, including the top parts of the inclined webs, has a plate thickness of 12 mm, whereas the bottom plate and the bottom parts of the webs are 8 mm thick. All stiffeners are made from 6-mm-thick steel plates welded to the skin plates. The effective cross-sectional properties of the girder under different pure section force configurations are shown in Table 4, where a negative sign indicates compression, and the axis system is indicated in Fig. 5. The effective plate thickness reduction due to buckling of plate fields is calculated based on column-like behavior according to Eurocode 3 [53].

Three stress points, which are indicated in Fig. 4, are investigated in the following sections. The effective cross-sectional properties critical for all three points are shown in Table 4, and the effective cross-sections are shown in Fig. 5.

4. Long-term extreme stresses in the Hardanger Bridge girder

4.1. Quarter-span detailed investigations

Stress point 2 in the quarter span of the bridge girder was chosen for detailed investigations of the long-term extreme stresses. Fig. 6 shows that the quarter span is critical since all section forces considered are relatively large. Stress point 2 is chosen because it is affected by all three section force processes considered, although the strong-axis moment dominates the total stresses.

4.1.1. Sectorial extreme stress investigations

The extreme stresses given the two defined wind directions, East and West, are calculated using the five methods shown in Table 5. The table outlines the theoretical basis and limitations of all methods in brief, and further details are provided in Section 2.

In Figs. 7 and 8, the 100-year return period long-term extreme response is investigated by considering two environmental variables at a time, for easterly and westerly winds, respectively. Here, the mean wind velocity together with one turbulence parameter at a time are described as stochastic variables. The turbulence parameters that are treated deterministically are chosen according to the point on the contour with the case of maximum mean wind velocity, as shown in Table 6. For illustration purposes, the turbulence parameters used in the design calculations of the bridge are also shown in the table. The Design Basis

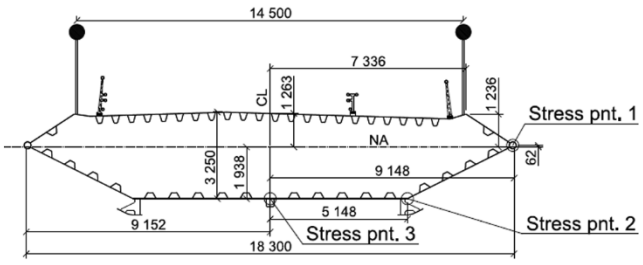

Fig. 4. The Hardanger Bridge girder cross-section.

mean wind velocity is significantly stronger than the full-scale measurements at the bridge midspan. Lystad et al. [39] concluded that the measuring mast used to establish the design basis for the Hardanger Bridge would likely overpredict the wind speed at the bridge midspan due to terrain wind speed-up effects at the mast position.

The 100-year return period environmental contour conditional on wind direction is shown together with the design point found by the IFORM and the ECM in Figs. 7 and 8. The design basis turbulence parameters are also indicated in the figures. In the background of the plots, the normalized contribution to the integral in Eq. (8) for the 100-year return period response is shown. The IFORM design point can be seen often to be located close to the maximum contribution to the FLM. Iso-response lines for the expected value of the short-term extreme stresses at stress point 2, as defined by Eq. (5), are shown in the figures as solid gray lines. The inclinations of these lines are indications of the stress sensitivity to the turbulence parameters.

The design stresses calculated by all methods are shown for different combinations of stochastically described turbulence parameters in Fig. 9 and Tables 7 and 8 for easterly and westerly winds, respectively. The FLM calculations become very computationally demanding when the number of dimensions becomes large, so these calculations are performed only for up to three-dimensional combinations. The expected value of the short-term extreme response from the ECM along with the correction factor, C_{corr}, and percentiles needed to correct the short-term ECM solution, p_{corr}, corresponding to the different long-term extreme response estimates are shown in Figs. 10 and 11 and Tables 7 and 8.

The stresses at stress point 2 are greatly affected by the along-wind turbulence standard deviation σ_u, so by describing this parameter and the mean wind velocity as stochastic variables, the long-term extreme stresses at stress point 2 can be estimated quite well. By also including the vertical turbulence standard deviation, the accuracy of the predicted long-term extreme response will improve even further.

Relatively small differences between the long-term extreme value prediction methods can be found in Fig. 9 and Tables 7 and 8, although the methods based on the approximate formulation in Eq. (10) are slightly unconservative, as expected. However, larger deviations can be seen between the methods for the westerly winds, especially for combinations including the along-wind turbulence standard deviation.

Kleiven and Haver [12] concluded that the relative effect of short-term extreme response uncertainty was reduced when the number of influential environmental parameters was increased. For the easterly winds, a similar trend is seen for the Hardanger Bridge buffeting response as well. When influential environmental parameters such as the along-wind turbulence standard deviation are described as stochastic variables, the difference between the expected short-term extreme response predicted by the ECM and the long-term extreme responses is reduced, as reflected by the reduced correction factors and percentiles in Figs. 10 and 11 and Tables 7 and 8. This is also the case for westerly winds when using long-term methods based on the approximate formulation in Eq. (10). However, this effect is not clear for westerly winds when using long-term methods based on exact formulations. The westerly wind Weibull distribution used in the investigations herein, established in [8], has a low shape parameter, k, indicating a long-tailed distribution. The contributions to the FLM shown in the background of Fig. 8 are farther out in the tail of the joint PDF than for the easterly winds. In this case, the IFORM design point is farther away from the area contributing the most to the FLM extreme response. These observations indicate that the accuracy of the approximate methods is sensitive to the tail shape of the environmental parameter joint PDF.

The long-term stresses in all three stress points are calculated using the IFORM Eq. (15) and are shown in Fig. 12. Large effects on the long-term extreme stresses can be observed by describing different turbulence parameters as stochastic variables. Stress point 1 does not receive significant contributions from weak-axis bending, and as a result, only the along-wind turbulence parameters significantly affect the long-term

Table 4
Effective cross-sectional properties of the Hardanger Bridge under pure section force configurations (NA-i refers to the neutral axis of the full cross-section, and NA_{eff}-i refers to the neutral axis of the effective cross-section).

A [m^2]	A_{eff} [m^2]	I_y [m^4]	$I_{y,eff}$ [m^4]	I_z [m^4]	$I_{z,eff}$ [m^4]	NA-y [m]	NA-z [m]	NA_{eff}-y [m]	NA_{eff}-z [m]	N	M_y	M_z
0.565	0.372	0.969	0.629	15.193	9.016	0.000	0.000	−0.035	0.105	−1	0	0
0.565	0.489	0.969	0.722	15.193	13.413	0.000	0.000	0.005	0.249	0	−1	0
0.565	0.489	0.969	0.854	15.193	12.131	0.000	0.000	−0.821	0.011	0	0	−1

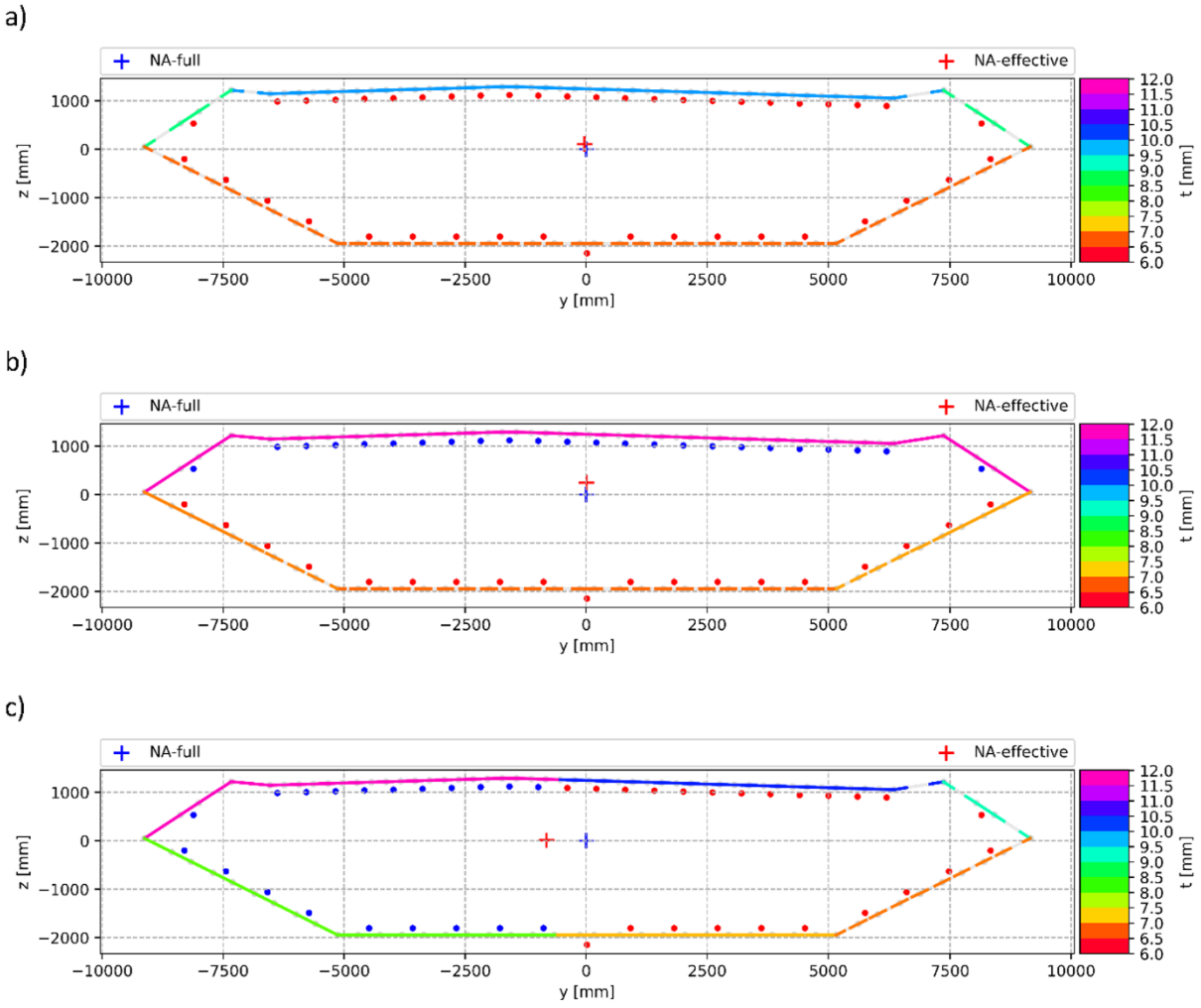

Fig. 5. Effective cross-sections for (a) pure axial compression (N = −1), (b) pure weak-axis bending with compression in the bottom plate (M_y = −1), and (c) pure strong-axis bending with compression on the right-hand side of the figure (M_z = −1). Effective thicknesses are indicated by the color bar, and the stiffener centroids are shown as red dots in compression and blue dots in tension. (For interpretation of the references to color in this figure legend, the reader is referred to the web version of this article.)

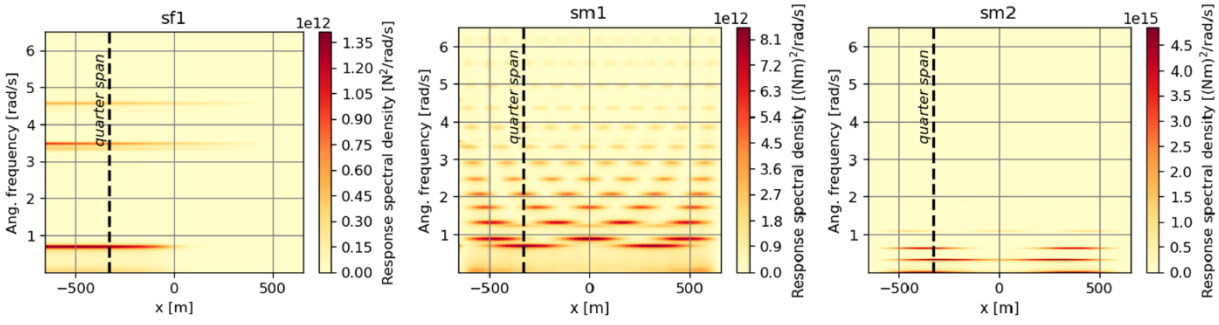

Fig. 6. Along-span response spectral density contour plots of the axial force (sf1), the weak-axis moment (sm1) and the strong-axis moment (sm2).

Table 5
Theoretical basis overview of considered extreme value methods.

	Full integration	Reliability method	Extreme response uncertainty	Exact formulation	Approx. formulation
FLM Eq. (8)	Yes	No	Yes	Yes	No
FLM Eq. (10)	Yes	No	Yes	No	Yes
IFORM Eq. (15)	No	Yes	Yes	No	Yes
IFORM Eq. (19)	No	Yes	Yes	Yes	No
ECM	No	Yes	No	No	No

Table 6
Deterministic turbulence parameters at girder height corresponding to the event of maximum mean wind velocity (contour tip and design basis values) [55].

Wind direction	U [m/s]	σ_u [m/s]	σ_w [m/s]	A_u	A_w	K_u	K_w
East	23.76	2.84	1.10	25.8	2.01	6.92	5.98
West	33.79	3.66	1.36	47.1	3.32	8.21	8.65
Design Basis	36.6	0.136U	0.068U	40.8	3.3	8.8	6.3

stresses. Stress point 3, however, is dominated by weak axis-bending, and the vertical turbulence parameters are more important to the estimated long-term stresses.

4.1.2. *Omnidirectional extreme stresses by the FLM*

The sectorial extreme response has been investigated thus far with a focus on methodology to estimate extreme stresses. However, the sectorial extreme response does not correspond directly to the omnidirectional extreme response.

The omnidirectional full long-term extreme response CDF can be calculated as a weighted sum of the CDFs conditional on wind direction [56]:

$$F_R(r) = \sum_i p_i F_{R|\theta}(r|\theta_i) \tag{37}$$

where p_i is the probability of the wind coming from sector θ_i. In general, the response CDF conditional on the wind direction needs to include the possible effects of skew winds. As mentioned in Section 3.1 and discussed in [8,39], the terrain surrounding the Hardanger Bridge channels the strong winds, so the two defined wind directions, East and West, can be considered to be perpendicular to the bridge.

In Table 9, the omnidirectional 100-year return period extreme stresses at stress point 2 are presented.

Estimating the omnidirectional extreme stresses using the environmental contour method and the IFORM, however, is not straightforward. Winterstein [56] suggested a simplified way to estimate a lower bound of the omnidirectional extreme response from sectorial subpopulations using the IFORM. Another method suggested by [56] was to fit a function to the tail of the long-term extreme response CDF based on IFORM extreme response estimates and use Eq. (37) to calculate the omnidirectional extreme response. Further, [57] and [58] estimated environmental contours by including the wind direction as a circular variable.

All these methods introduce some limitations and uncertainties, and the appropriate choice will be problem-specific. Such methods have not been investigated in the work presented here but to obtain omnidirectional design stresses, the directionality of the wind must be considered.

As seen in Table 9, with one wind direction dominating the response, the sectorial extreme response will be a conservative choice for the omnidirectional extreme response and could be a reasonable design value in some cases.

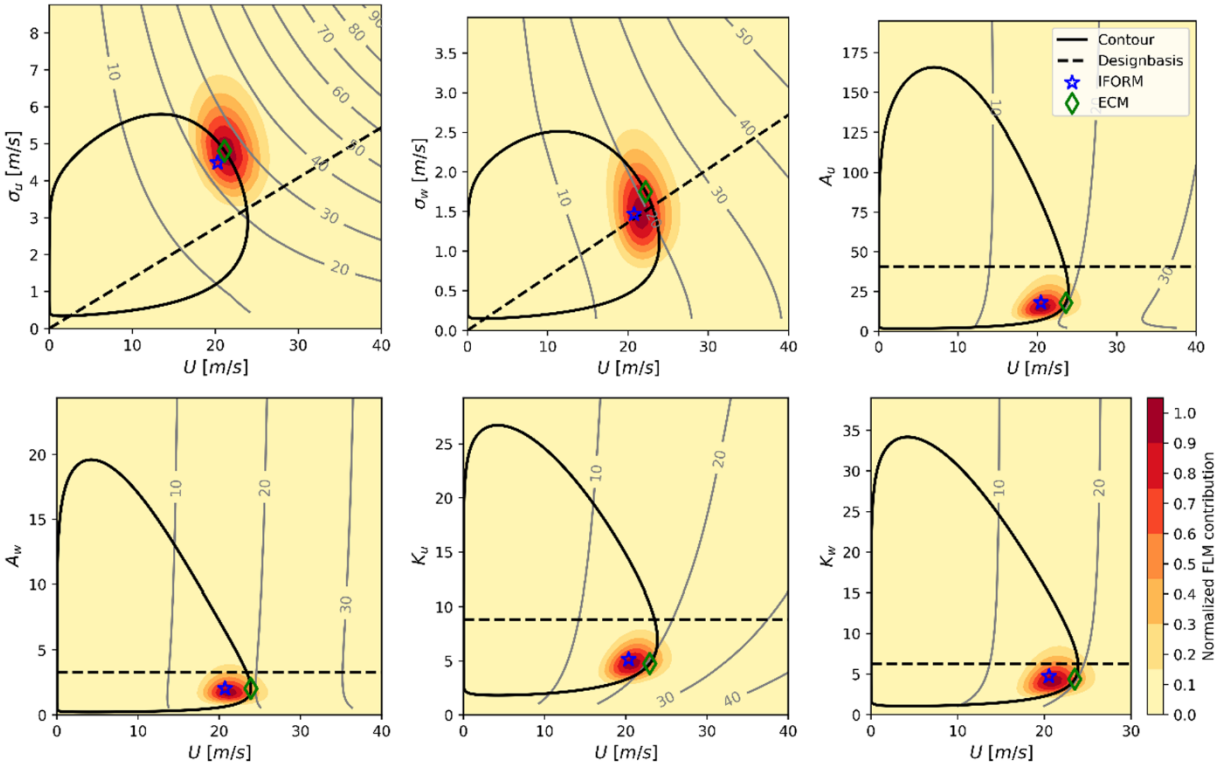

Fig. 7. Long-term extreme girder stresses at the quarter span in stress point 2 from easterly winds. The normalized contribution to the 100-year return period extreme value using the FLM is shown in the background, and the IFORM and the ECM design point are indicated.

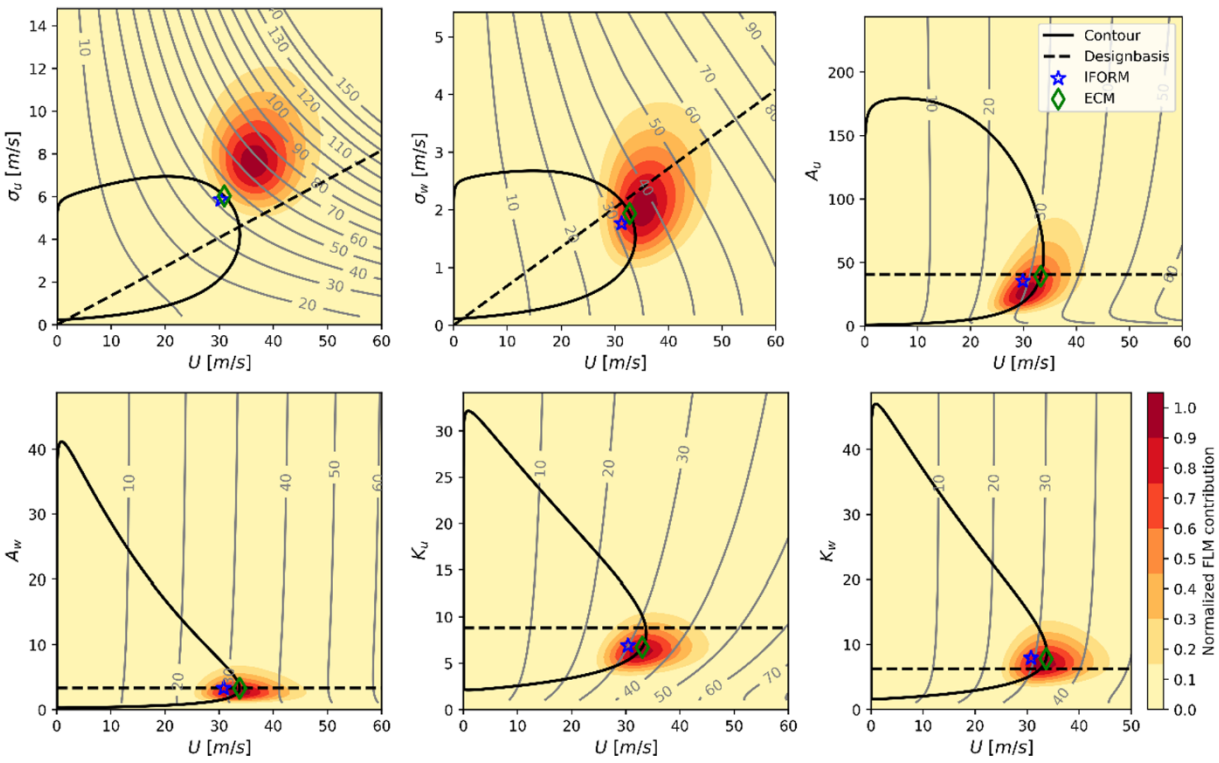

Fig. 8. Long-term extreme girder stresses at the quarter span in stress point 2 from westerly winds. The normalized contribution to the 100-year return period extreme value using the FLM is shown in the background, and the IFORM and the ECM design point are indicated.

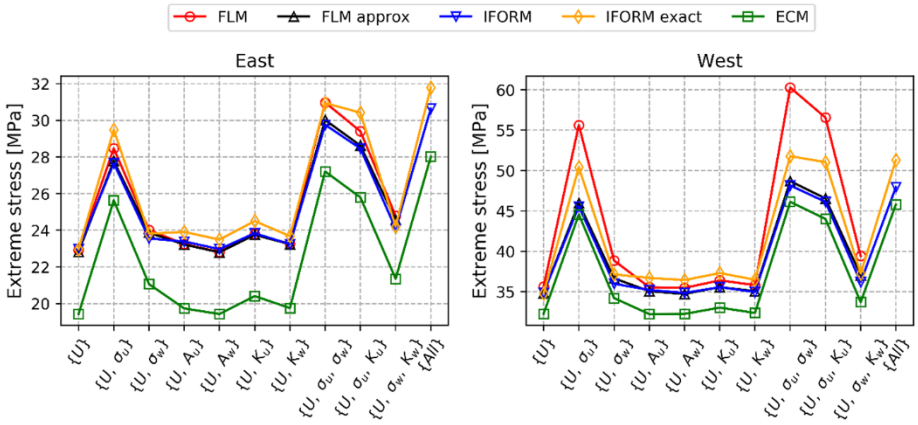

Fig. 9. Extreme girder stresses in stress point 2 at the quarter span, considering different combinations of turbulence parameters described as random variables.

4.2. Along-span investigations

In the previous sections, detailed investigations of the girder quarter span were presented. However, the bridge behavior can change along the span. In the following, the design point for the girder stresses conditional on the two wind directions is calculated along the span using the IFORM Eq. (15) and the ECM.

In Fig. 13, the stresses in the three stress points under consideration are plotted along the bridge span for easterly and westerly winds. In these calculations, all turbulence parameters are treated as stochastic variables. The 100-year return period long-term extreme stresses calculated by the IFORM are shown together with the expected short-term extreme response calculated by the ECM. The ECM correction factor and the short-term extreme response distribution percentile corresponding to the IFORM long-term stresses are shown in Fig. 13. Some variations in the correction factors and percentiles are seen along the span and between the different stress points, although the variations are relatively small.

In Figs. 14 and 15, the along-span variations in the turbulence parameters corresponding to the ECM design point are shown for the easterly and westerly winds, respectively. In general, small variations in the critical turbulence parameter combinations can be seen, below $\pm$ 6%. However, for the most influential turbulence parameters, even less variation is seen. Assuming that stress point 1 is affected only by the along-wind turbulence parameters such as σ_u, A_u and K_u, the variation in the critical turbulence parameter combinations is typically under $\pm$ 1%. This case is also pertinent when considering stress point 3, which is dominated by weak axis bending and thus sensitive to vertical turbulence, with a slight exception for the A_w parameter.

Based on these observations, a reasonable estimate for the long-term extreme response at all positions along the Hardanger Bridge girder could be achieved by the following simplified approach:

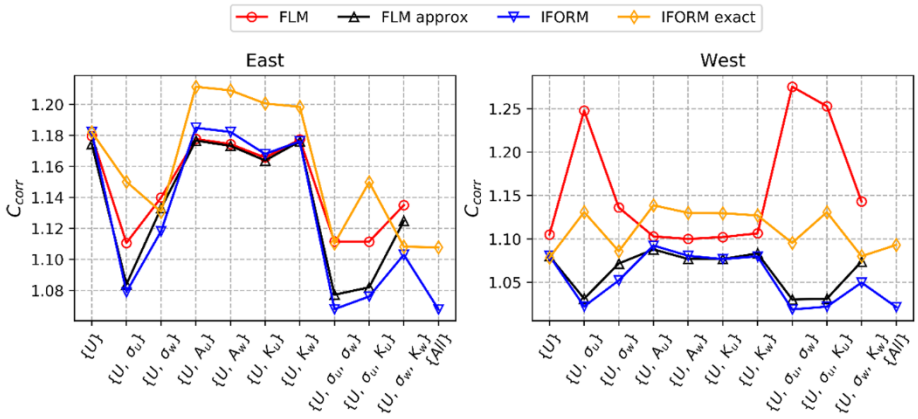

Fig. 10. Long-term correction factors (long-term/ECM) for the girder stresses in stress point 2 at quarter span, considering different combinations of turbulence parameters described as random variables.

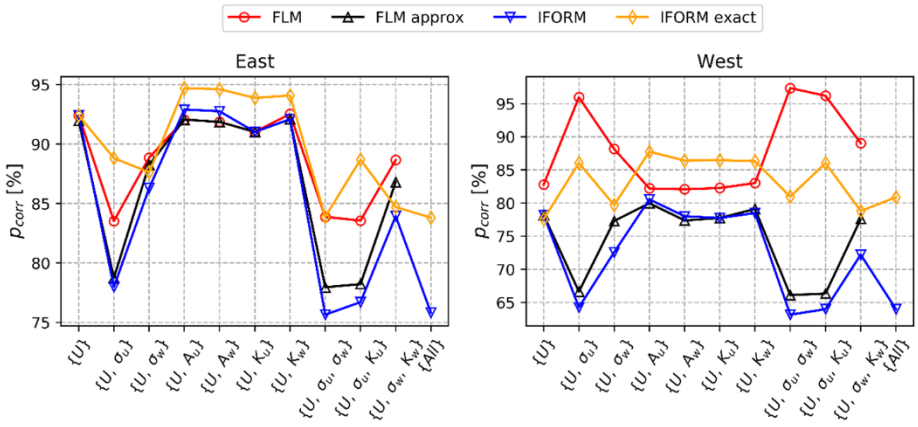

Fig. 11. ECM short-term extreme value CDF percentile corresponding to the long-term extreme girder stresses in stress point 2 at quarter span, considering different combinations of turbulence parameters described as random variables.

Table 7
Extreme stresses, correction factors and short-term percentiles for long-term correction of the ECM solution at quarter span in stress point 2 for easterly winds. Stresses from different long-term methods and combinations of turbulence parameters described as random variables are presented.

Included variables, **w**		$\{U\}$	$\{U, \sigma_u\}$	$\{U, \sigma_w\}$	$\{U, A_u\}$	$\{U, A_w\}$	$\{U, K_u\}$	$\{U, K_w\}$	$\{U, \sigma_u, \sigma_w\}$	$\{U, \sigma_u, K_u\}$	$\{U, \sigma_w, K_w\}$	$\{All\}$
Extreme response *[Mpa]*	FLM Eq. (8)	22.9	28.5	24.0	23.2	22.8	23.8	23.3	31.0	29.4	24.8	N/A
	FLM Eq. (10)	22.8	27.8	23.9	23.2	22.8	23.8	23.2	30.0	28.6	24.6	N/A
	IFORM Eq. (15)	23.0	27.7	23.6	23.4	23.0	23.8	23.2	29.8	28.5	24.1	30.6
	IFORM Eq. (19)	23.0	29.5	23.8	23.9	23.5	24.5	23.7	30.9	30.4	24.2	31.8
	ECM	19.4	25.6	21.1	19.7	19.4	20.4	19.8	27.2	25.8	21.4	28.0
C_{corr}	FLM Eq. (8)	1.18	1.11	1.14	1.18	1.17	1.17	1.18	1.11	1.11	1.13	N/A
p_{corr} *[%]*	FLM Eq. (8)	92	84	89	92	92	91	93	84	84	89	N/A

Table 8
Extreme stresses, correction factors and short-term percentiles for long-term correction of the ECM solution at quarter span in stress point 2 for westerly winds. Stresses from different long-term methods and combinations of turbulence parameters described as random variables are presented.

Included variables, **w**		$\{U\}$	$\{U, \sigma_u\}$	$\{U, \sigma_w\}$	$\{U, A_u\}$	$\{U, A_w\}$	$\{U, K_u\}$	$\{U, K_w\}$	$\{U, \sigma_u, \sigma_w\}$	$\{U, \sigma_u, K_u\}$	$\{U, \sigma_w, K_w\}$	$\{All\}$
Extreme response *[Mpa]*	FLM Eq. (8)	35.6	55.6	38.9	35.5	35.5	36.4	35.8	60.3	56.6	39.4	N/A
	FLM Eq. (10)	34.8	46.0	36.7	35.1	34.7	35.6	35.1	48.7	46.5	37.0	N/A
	IFORM Eq. (15)	34.8	45.6	36.0	35.2	34.8	35.6	35.0	48.2	46.1	36.2	47.9
	IFORM Eq. (19)	34.8	50.4	37.1	36.7	36.4	37.3	36.5	51.8	51.0	37.2	51.3
	ECM	32.3	44.6	34.2	32.2	32.3	33.0	32.4	46.1	44.0	33.7	45.8
C_{corr}	FLM Eq. (8)	1.11	1.25	1.14	1.10	1.10	1.10	1.11	1.28	1.25	1.14	N/A
p_{corr} *[%]*	FLM Eq. (8)	83	96	88	82	82	82	83	97	96	89	N/A

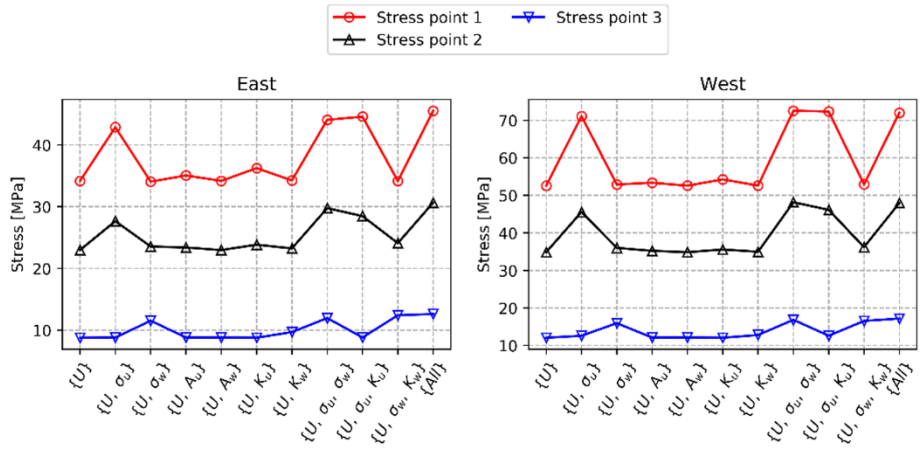

Fig. 12. Long-term extreme girder stresses at quarter span in all considered stress points, identified by the IFORM EQ.

Table 9
Omnidirectional 100-year return period extreme stresses at quarter span at stress point 2 for westerly winds. Combinations of stochastically described turbulence parameters are presented.

Included variables, **w**	$\{U\}$	$\{U, \sigma_u\}$	$\{U, \sigma_w\}$	$\{U, A_u\}$	$\{U, A_w\}$	$\{U, K_u\}$	$\{U, K_w\}$	$\{U, \sigma_u, \sigma_w\}$	$\{U, \sigma_u, K_u\}$	$\{U, \sigma_w, K_w\}$
FLM East	22.9	28.4	24.0	23.2	22.8	23.8	23.3	31.0	29.4	24.8
FLM West	35.6	55.8	38.9	35.5	35.4	36.4	35.8	60.3	56.6	39.4
FLM Omni	33.5	49.4	36.1	33.6	33.4	34.2	33.7	53.4	50.1	36.6

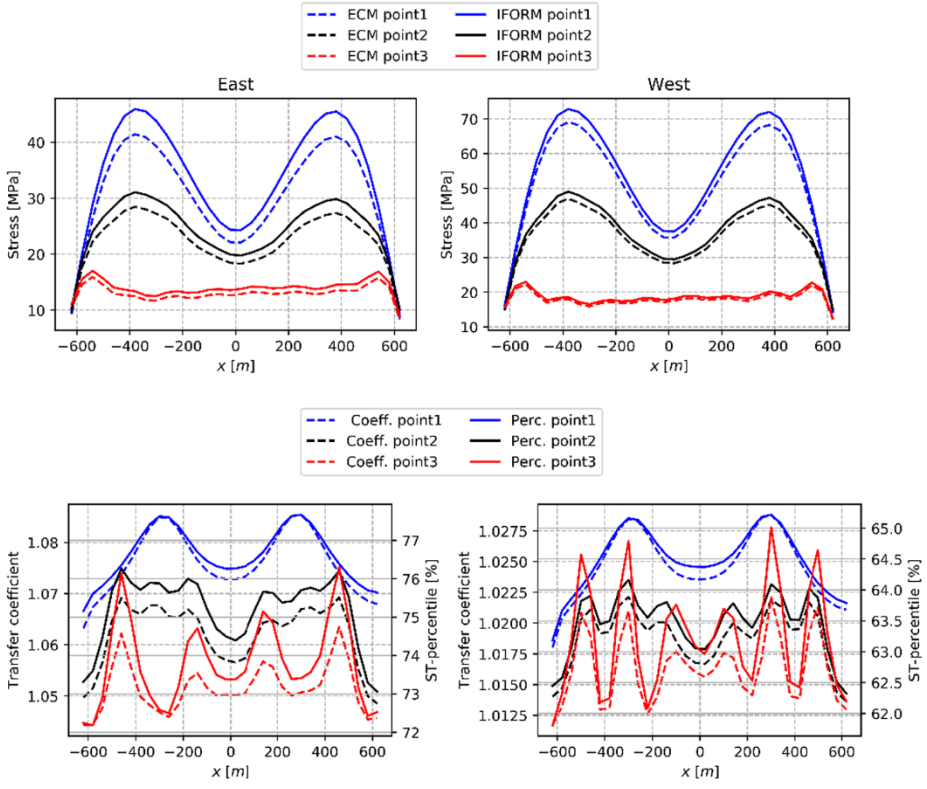

Fig. 13. Along-span stresses and correction factors and short-term extreme CDF percentiles from the ECM and the IFORM. Left; easterly winds, right; westerly winds.

1. Calculate the critical environmental parameter combinations in a representative section along the girder using the ECM.
2. Calculate the correction factor or the short-term extreme value distribution percentile corresponding to the long-term extreme value in the section considered.
3. Calculate the short-term response in all sections along the girder based on the critical turbulence parameter combination identified by the ECM in 1.
4. Correct the short-term response along the span with the correction identified in 2.

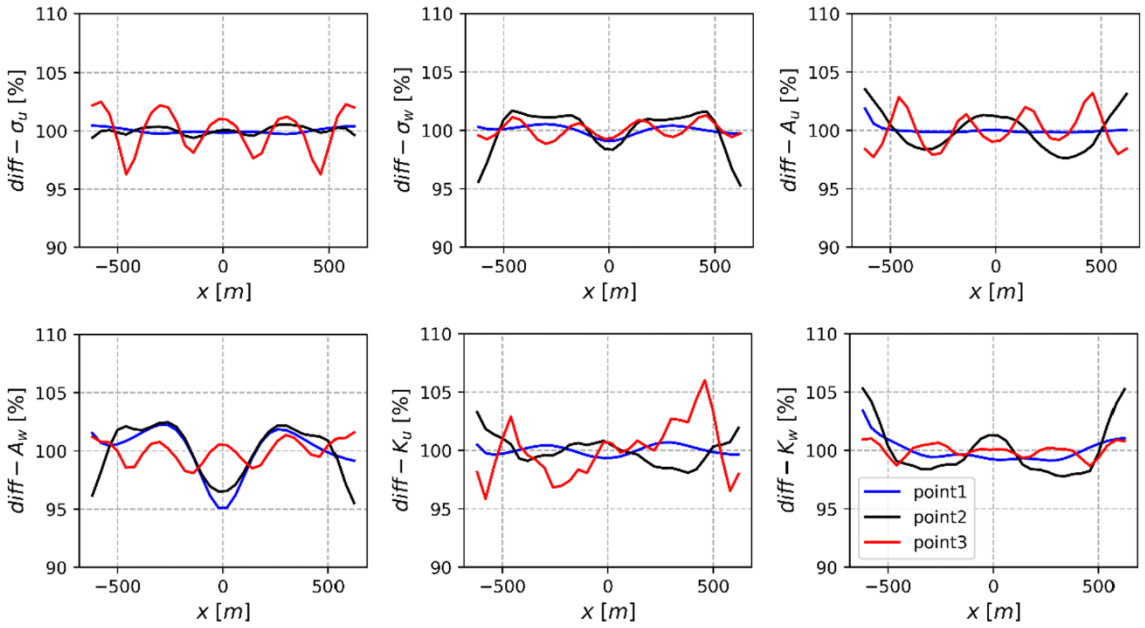

Fig. 14. Percentage of along-span mean critical turbulence variable identified by the ECM design point for easterly winds. diff-w_i = 100% * $w_i(x)$/mean(w_i).

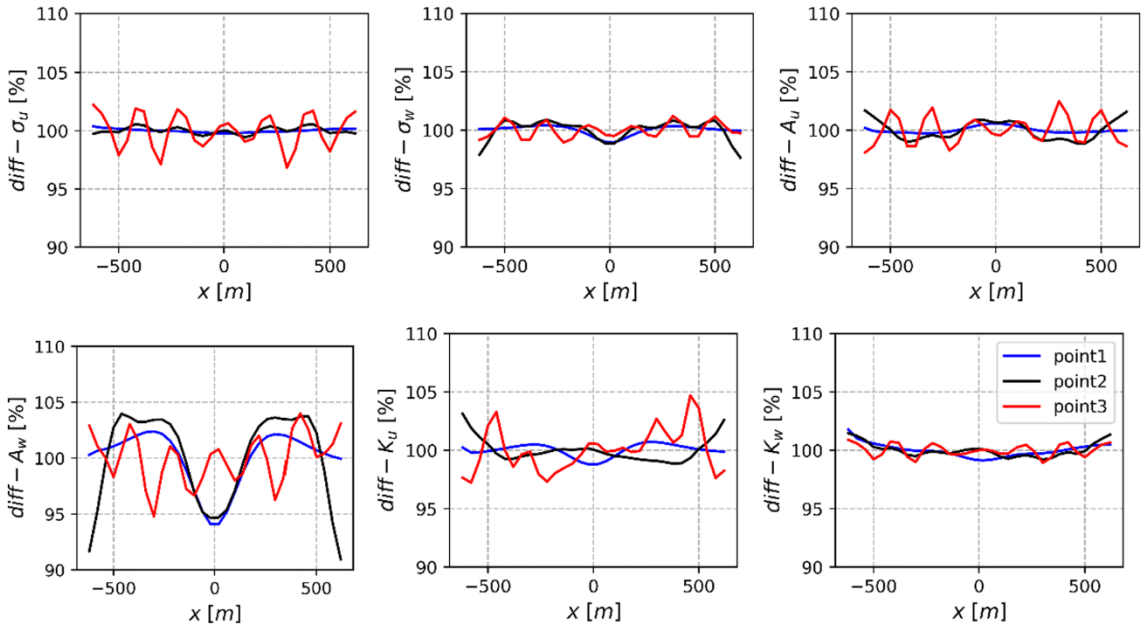

Fig. 15. Percentage of along-span mean critical turbulence variable identified by the ECM design point for westerly winds. diff-w_i = 100% * $w_i(x)$/mean(w_i).

5. Comparison with full-scale acceleration peak response measurements

Fenerci et al. [59] found that the buffeting acceleration response measured at full scale at the Hardanger Bridge was very scattered when plotted as function of the mean wind velocity. They concluded that most of the scattered data could be explained by the uncertainty in the turbulence field. In Fig. 16, the midspan peak acceleration measurements from the Hardanger Bridge are shown for lateral, vertical and torsional motions. The 10-minute maximum peaks are plotted, and the high-frequency content above 1 Hz is removed by low-pass filtering of the measurements. The measurement data are colored by the normalized scatter density multiplied by the mean wind velocity squared. The measurements are split into easterly and westerly wind directions, but the measurements for the opposite direction are shown as gray scatter in the background of the plot. The data from the full-scale measurement program at the Hardanger Bridge site is available with open access [60,61] and the measurement system is described in detail in [59].

To investigate the performance of the long-term extreme response analyses, the long-term acceleration response at the midspan of the Hardanger Bridge girder is calculated and compared with the full-scale measurements. The acceleration response has a different behavior than the design stresses which has been the focus in the previous parts of this paper, but the acceleration response comparison can provide an indication of the performance of the overall methodology.

The 100-year return period extreme accelerations estimated by the classical IFORM and the ECM, conditional on the mean wind velocity, are also shown in Fig. 16. A simple modification to the iteration algorithm shown in Eq. (27) is needed to solve the IFORM problem when the mean wind velocity is given. The modification reads:

$$\boldsymbol{u}^{k+1} = \sqrt{\beta^2 - u_1^2}\,\frac{\nabla \breve{r}_n(\boldsymbol{u}^k)}{\left|\nabla \breve{r}_n(\boldsymbol{u}^k)\right|} \tag{38}$$

where u_1 is the standard normal variable corresponding to the given mean wind velocity, n is the number of environmental variables and k indicates the iteration number. Since the short-term extreme value uncertainty is not included as a variable in the ECM, the expression above reduces to:

$$\boldsymbol{u}^{k+1} = \sqrt{\beta^2 - u_1^2}\,\frac{\nabla \breve{r}_{n-1}(\boldsymbol{u}^k)}{\left|\nabla \breve{r}_{n-1}(\boldsymbol{u}^k)\right|} \tag{39}$$

As Fig. 16 shows, the extreme accelerations predicted by the IFORM and the ECM correspond quite well with the upper bound of the full-scale measurement data. The extreme responses are calculated based on a 100-year return period, and the full-scale data are based on approximately 4 years of measurements, so theoretically, the measurements should all fall within the extreme response predicted with the IFORM. For illustration purposes, the expected value of the short-term extreme response calculated using the design basis turbulence parameters is also indicated in Fig. 16.

In general, uncertainties regarding static force coefficients for the different bridge members and limitations in the turbulence model can affect the comparison. For the lateral acceleration response, the calculations correspond quite well with the measurements, although some events fall well outside the extreme predictions. Some of the most profound uncertainties for the lateral response are the assumption of stationarity and the estimated static drag coefficients for the girder and the other bridge members.

When considering the vertical response, a kink in the predicted extreme response line can be observed at approximately 11 m/s. The vertical response is strongly influenced by the aerodynamic derivatives. The value of 11 m/s corresponds to the reduced velocity where the first vertical frequency falls within the experimental test range of the AD, as shown in [8]. Since the fitted model for the AD is not smooth in the transition between the experimental data range and the extrapolated area, this is reflected in the predicted extreme acceleration response.

When considering the torsional acceleration, the predicted extreme responses seem to be farther out in the tail of the measured scatter than

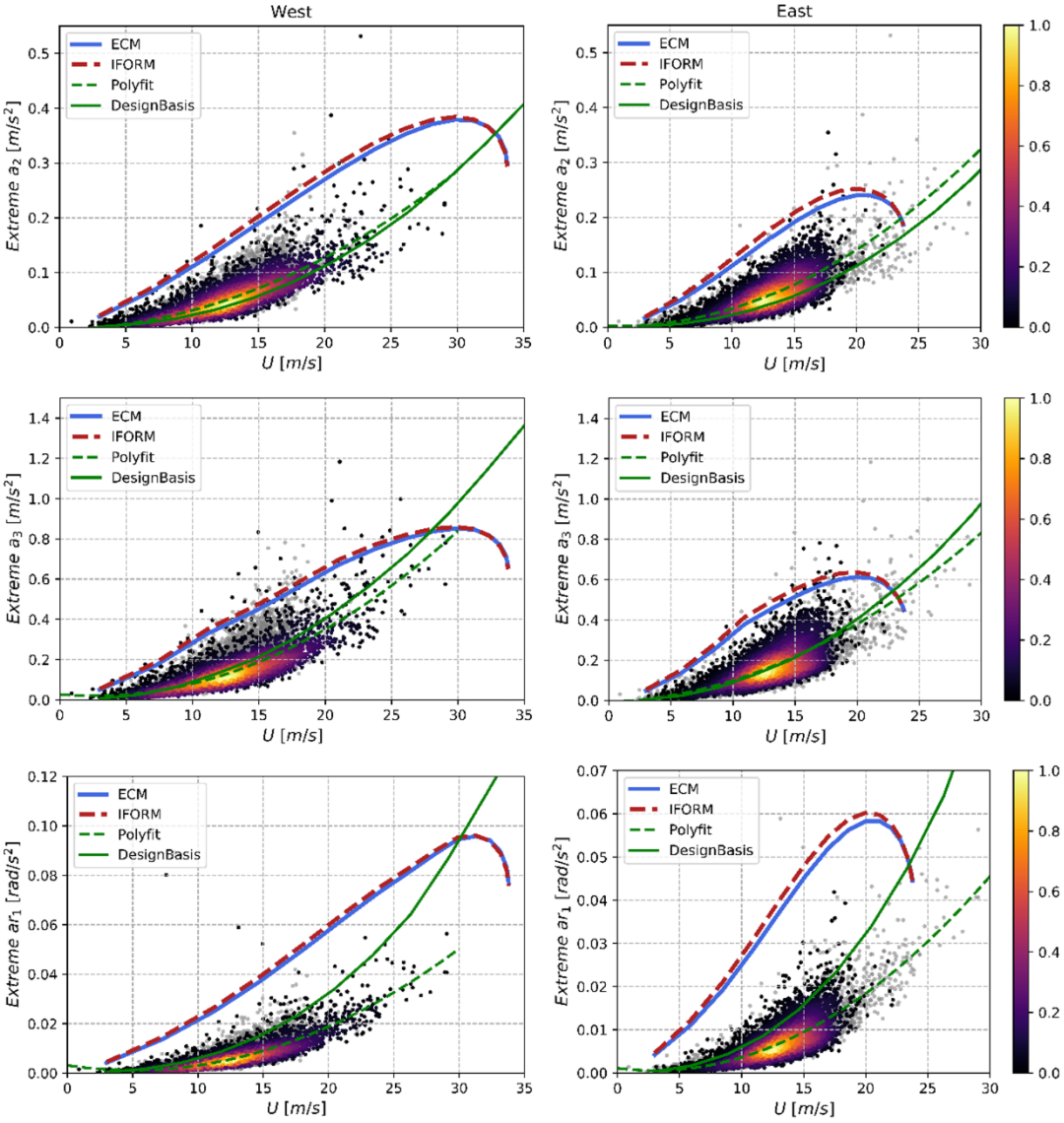

Fig. 16. Lateral- (a2), vertical- (a3) and torsional (ar1) peak acceleration responses of the Hardanger Bridge midspan, established by full-scale measurements (scattered data points colored by scatter density multiplied by the mean wind velocity squared, opposite wind direction indicated as gray data), the ECM and the IFORM conditional on mean wind velocity, the design basis turbulence parameters and a 2nd-order polynomial fit to the measured data.

the other acceleration components. The acceleration response is dominated by higher frequencies than the lateral and vertical responses, so neglecting aerodynamic admittance may significantly affect the torsional response. The first torsional mode is outside the reduced velocity experimental test range for all mean wind velocities below ~ 28 m/s, so almost all the predictions are based on aerodynamic damping and stiffness in the extrapolated range.

In Fig. 17, the short-term peak factor is shown for the measured data, plotted in the same way as in Fig. 16. The predicted peak factors from the design basis analyses are also indicated, corresponding very well with the polynomial fit to the full-scale data. However, the full-scale measured peak factors are very scattered, which is an illustration of the uncertainty in the short-term extreme peak response.

6. Conclusions

The long-term extreme response of the Hardanger Bridge considering uncertain turbulence parameters has been investigated. Considerable effects on the predicted extreme values relevant for design purposes were found, indicating a need to revisit the design methodology used for long-span bridges subjected to turbulent wind loading. In brief, the following conclusions are drawn:

- Extreme design stresses were predicted directly from the frequency-domain buffeting analyses.
- The turbulence uncertainty has large effects on the predicted extreme design stresses of the Hardanger Bridge. Treating the turbulence parameters as deterministic variables may introduce significant errors to the estimated extreme stresses.
- Uncertainty in the short-term extreme response should be considered when predicting extreme stresses for design purposes.
- Reliability-based methods such as the inverse first-order reliability method (IFORM) and the environmental contour method (ECM)

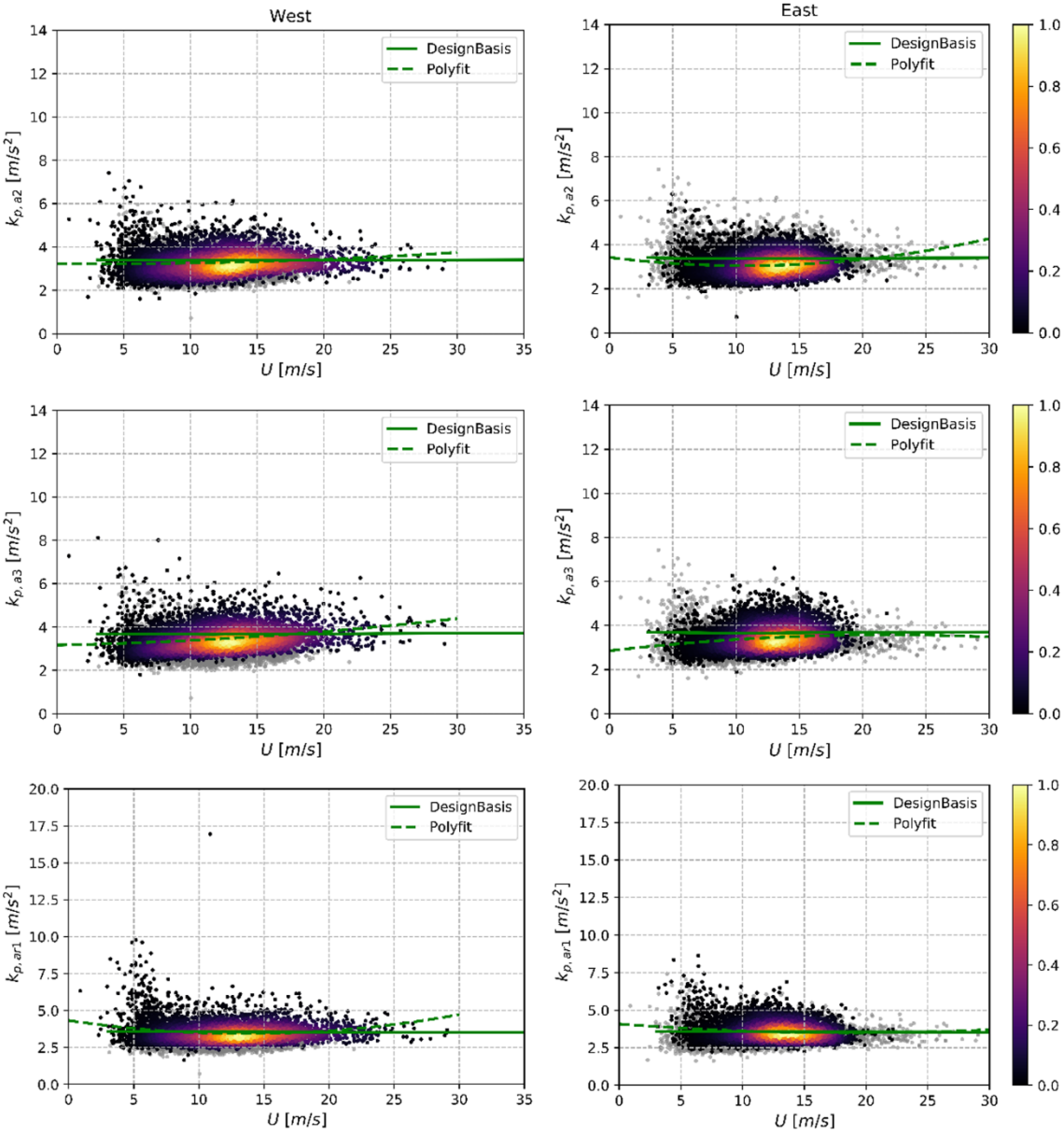

Fig. 17. Lateral- (a2), vertical- (a3) and torsional (ar1) short-term peak factors for the acceleration responses of the Hardanger Bridge midspan. The full-scale measurements are shown (scattered data points colored by scatter density multiplied by the mean wind velocity squared, opposite wind direction indicated as gray data) together with the peak factors estimated by the buffeting analyses using the design basis turbulence parameters. In addition, a 2nd-order polynomial fit to the measured data is shown.

become less effective than full long-term methods when many sections along a long-span bridge need to be assessed.
- With one wind direction dominating the response, the sectorial extreme response could be a reasonable conservative choice for the omnidirectional extreme response in some cases.
- Relatively small variations in the critical turbulence parameter combinations predicted by the ECM were found along the span of the Hardanger Bridge.
- The long-term methods IFORM and ECM were able to predict the variability in the scattered extreme peak acceleration response measured at full scale at the Hardanger Bridge, displaying significant improvement compared with the methodology used for the design of the bridge.

CRediT authorship contribution statement

Tor M. Lystad: Conceptualization, Methodology, Software, Formal analysis, Writing - original draft, Writing - review & editing, Visualization. **Aksel Fenerci:** Validation, Investigation, Data curation. **Ole Øiseth:** Conceptualization, Supervision, Project administration.

Declaration of Competing Interest

The authors declare that they have no known competing financial interests or personal relationships that could have appeared to influence the work reported in this paper.

Acknowledgements

Funding: The research presented in this paper has been financed by Norconsult AS, the Norwegian Public Roads Administration (NPRA) and the Research Council of Norway.

References

[1] Brownjohn JMW, Bocciolone M, Curami A, Falco M, Zasso A. Humber bridge full-scale measurement campaigns 1990–1991. J Wind Eng Ind Aerodyn 1994;52:185–218. https://doi.org/10.1016/0167-6105(94)90047-7.
[2] Miyata T, Yamada H, Katsuchi H, Kitagawa M. Full-scale measurement of Akashi-Kaikyo Bridge during typhoon. J Wind Eng Ind Aerodyn 2002;90:1517–27. https://doi.org/10.1016/S0167-6105(02)00267-2.
[3] Macdonald JHG. Evaluation of buffeting predictions of a cable-stayed bridge from full-scale measurements. J Wind Eng Ind Aerodyn 2003;91:1465–83. https://doi.org/10.1016/J.JWEIA.2003.09.009.
[4] Wang H, Asce M, Tao T, Asce SM, Gao Y, Xu F. Measurement of wind effects on a kilometer-level cable-stayed bridge during Typhoon Haikui. J Struct Eng 2018;144:1–23. https://doi.org/10.1061/(ASCE)ST.1943-541X.0002138.
[5] Wang H, Li A, Guo T, Xie J. Field measurement on wind characteristic and buffeting response of the Runyang Suspension Bridge during typhoon Matsa. Sci China, Ser E Technol Sci 2009;52:1354–62. https://doi.org/10.1007/s11431-008-0238-y.
[6] Cheynet E, Bogunovic Jakobsen J, Snæbjörnsson J. Buffeting response of a suspension bridge in complex terrain. Eng Struct 2016;128:474–87. https://doi.org/10.1016/J.ENGSTRUCT.2016.09.060.
[7] Meng X, Nguyen DT, Xie Y, Owen JS, Psimoulis P, Ince S, et al. Design and implementation of a new system for large bridge monitoring—geoshm. Sensors 2018:18. https://doi.org/10.3390/s18030775.
[8] Lystad TM, Fenerci A, Øiseth O. Buffeting response of long-span bridges considering uncertain turbulence parameters using the environmental contour method. Eng Struct 2020;213:110575. https://doi.org/10.1016/J.ENGSTRUCT.2020.110575.
[9] Fenerci A, Øiseth O. Measured buffeting response of a long-span suspension bridge compared with numerical predictions based on design wind spectra. J Struct Eng 2017;143.. https://doi.org/10.1061/(ASCE)ST.1943-541X.0001873.
[10] Dunham KK. Coastal highway route E39 – extreme crossings. Transp Res Procedia 2016;14:494–8. https://doi.org/10.1016/J.TRPRO.2016.05.102.
[11] Xu Y, Øiseth O, Moan T, Naess A. Prediction of long-term extreme load effects due to wave and wind actions for cable-supported bridges with floating pylons. Eng Struct 2018;172:321–33. https://doi.org/10.1016/J.ENGSTRUCT.2018.06.023.
[12] Kleiven G, Haver S. Met-ocean contour lines for design; correction for omitted variability in the response process. Proc. Fourteenth Int. Offshore Polar Eng. Conf., vol. 1, 2004, p. 202–10.
[13] Haver S, Kleiven G. Environmental contour lines for design purposes: why and when? 23rd Int. Conf. Offshore Mech. Arct. Eng. Vol. 1, Parts A B, 2004, p. 337–45. https://doi.org/10.1115/OMAE2004-51157.
[14] Norwegian Technology Standards Institution. NORSOK N-003 Actions and Action Effects. Oslo, Norway; 2007.
[15] Naess A, Moan T. Stochastic dynamics of marine structures. Cambridge University Press; 2013. https://doi.org/10.1017/CBO9781139021364.
[16] Sagrilo LVS, Naess A, Doria AS. On the long-term response of marine structures. Appl Ocean Res 2011;33:208–14. https://doi.org/10.1016/J.APOR.2011.02.005.
[17] Li H, Foschi RO. An inverse reliability method and its application. Struct Saf 1998;20:257–70. https://doi.org/10.1016/S0167-4730(98)00010-1.
[18] Der Kiureghian A, Zhang Y, Li C-C. Inverse reliability problem. J Eng Mech 1994;120:1154–9.
[19] Winterstein SR, Haver S. Environmental parameters for extreme response : inverse FORM with omission factors. Proc 6th Int. Conf Struct. Saf. Reliab., Innsbruck, Austria; 1993.
[20] Davenport AG. The relationship of reliability to wind loading. J Wind Eng Ind Aerodyn 1983;13:3–27. https://doi.org/10.1016/0167-6105(83)90125-3.
[21] Kareem A. Aerodynamic response of structures with parametric uncertainties. Struct Saf 1988;5:205–25. https://doi.org/10.1016/0167-4730(88)90010-0.
[22] Zhang L, Li J, Peng Y. Dynamic response and reliability analysis of tall buildings subject to wind loading. J Wind Eng Ind Aerodyn 2008;96:25–40. https://doi.org/10.1016/J.JWEIA.2007.03.001.
[23] Pagnini LC, Solari G. Gust buffeting and turbulence uncertainties. J Wind Eng Ind Aerodyn 2002;90:441–59. https://doi.org/10.1016/S0167-6105(01)00202-1.
[24] Pagnini L. Reliability analysis of wind-excited structures. J Wind Eng Ind Aerodyn 2010;98:1–9. https://doi.org/10.1016/J.JWEIA.2009.08.010.
[25] Seo D, Caracoglia L. Statistical buffeting response of flexible bridges influenced by errors in aeroelastic loading estimation. J Wind Eng Ind Aerodyn Wind Eng Ind Aerodyn 2012;104–106:129–40. https://doi.org/10.1016/j.jweia.2012.03.036.
[26] Seo D, Caracoglia L. Estimating life-cycle monetary losses due to wind hazards: Fragility analysis of long-span bridges. Eng Struct 2013;56:1593–606. https://doi.org/10.1016/j.engstruct.2013.07.031.
[27] Caracoglia L. Influence of uncertainty in selected aerodynamic and structural parameters on the buffeting response of long-span bridges. J Wind Eng Ind Aerodyn 2008;96:327–44. https://doi.org/10.1016/j.jweia.2007.08.001.
[28] Solari G, Piccardo G. Probabilistic 3-D turbulence modeling for gust buffeting of structures. Probabilistic Eng Mech 2001;16:73–86. https://doi.org/10.1016/S0266-8920(00)00010-2.
[29] Wu J, Chen SR. Probabilistic dynamic behavior of a long-span bridge under extreme events. Eng Struct 2011;33:1657–65. https://doi.org/10.1016/j.engstruct.2011.02.002.
[30] Vallis MB, Loredo-Souza AM, Ferreira V, Nascimento EL. Journal of Wind Engineering & Industrial Aerodynamics Classification and identification of synoptic and non-synoptic extreme wind events from surface observations in South America. R. J Wind Eng Ind Aerodyn 2019;193. https://doi.org/10.1016/j.jweia.2019.103963.
[31] Owen JS, Nguyen DT, Meng X, Psimoulis P, Xie Y. An observation of non-stationary response to non-synoptic wind on the Forth Road Bridge. J Wind Eng Ind Aerodyn 2020;206. https://doi.org/10.1016/j.jweia.2020.104389.
[32] Fenerci A, Øiseth O. Strong wind characteristics and dynamic response of a long-span suspension bridge during a storm. J Wind Eng Ind Aerodyn 2018;172:116–38. https://doi.org/10.1016/j.jweia.2017.10.030.
[33] Naess A. Technical note: On the long-term statistics of extremes. Appl Ocean Res 1984;6:227–8. https://doi.org/10.1016/0141-1187(84)90061-0.
[34] Borgman LE. Probabilities for heighest wave in hurricane. J Waterw Harb Coast Eng 1973;99:185–207.
[35] Giske F-IG, Leira BJ, Øiseth O. Full long-term extreme response analysis of marine structures using inverse FORM. Probabilistic Eng Mech 2017;50:1–8. https://doi.org/10.1016/J.PROBENGMECH.2017.10.007.
[36] Madsen HO, Krenk S, Lind NC. Methods of structural safety. New York: Dover Publications; 1986.
[37] Rosenblatt M. Remarks on a multivariate transformation. Ann Math Stat 1952;23:470–2.
[38] Fenerci A, Øiseth O. Site-specific data-driven probabilistic wind field modeling for the wind-induced response prediction of cable-supported bridges. J Wind Eng Ind Aerodyn 2018;181:161–79. https://doi.org/10.1016/J.JWEIA.2018.09.002.
[39] Lystad TM, Fenerci A, Øiseth O. Evaluation of mast measurements and wind tunnel terrain models to describe spatially variable wind field characteristics for long-span bridge design. J Wind Eng Ind Aerodyn 2018;179:558–73. https://doi.org/10.1016/J.JWEIA.2018.06.021.
[40] Kaimal J, Wyngaard J, Izumi Y, Coté OR. Spectral characteristics of surface-layer turbulence. Q J R Meteorol Soc 1972;98.
[41] Davenport AG. The spectrum of horizontal gustiness near the ground in high winds. Q J R Meteorol Soc 1961;87:194–211. https://doi.org/10.1002/qj.49708737208.
[42] Chen X, Kareem A, Matsumoto M. Multimode coupled flutter and buffeting analysis of long span bridges. J Wind Eng Ind Aerodyn 2001;89:649–64. https://doi.org/10.1016/S0167-6105(01)00064-2.
[43] Jain A, Jones NP, Scanlan RH. Coupled flutter and buffeting analysis. J Struct Eng 1996;122:716–25. https://doi.org/10.1061/(ASCE)0733-9445(1996)122:7(716).
[44] Jain A, Jones NP, Scanlan RH. Coupled aeroelastic and aerodynamic response analysis of long-span bridges. J Wind Eng Ind Aerodyn 1996;60:69–80. https://doi.org/10.1016/0167-6105(96)00024-4.
[45] Øiseth O, Rönnquist A, Sigbjörnsson R. Simplified prediction of wind-induced response and stability limit of slender long-span suspension bridges, based on modified quasi-steady theory: A case study. J Wind Eng Ind Aerodyn 2010;98:730–41. https://doi.org/10.1016/j.jweia.2010.06.009.

[46] Katsuchi H, Jones NP, Scanlan RH, Akiyama H. Multi-mode flutter and buffeting analysis of the Akashi-Kaikyo bridge. J Wind Eng Ind Aerodyn 1998;77–78: 431–41. https://doi.org/10.1016/S0167-6105(98)00162-7.
[47] Dassault Systèmes Simulia. ABAQUS 2018.
[48] Zhou S-J. Finite beam element considering shear-lag effect in box girder. J Eng Mech 2010;136:1115–22. https://doi.org/10.1061/(asce)em.1943-7889.0000156.
[49] Zhang Y-H, Lin L-X. Shear lag analysis of thin-walled box girders based on a new generalized displacement. Eng Struct 2014;61:73–83. https://doi.org/10.1016/j.engstruct.2013.12.031.
[50] Siedziako B, Øiseth O, Rønnquist A. An enhanced forced vibration rig for wind tunnel testing of bridge deck section models in arbitrary motion. J Wind Eng Ind Aerodyn 2017;164:152–63. https://doi.org/10.1016/J.JWEIA.2017.02.011.
[51] Standard Norge. Eurocode 1: Actions on structures - Part 1–4: General actions. Wind actions 2009.
[52] Strømmen E. Theory of bridge aerodynamics. Second edi. Springer; 2010.
[53] Standard Norge. Eurocode 3: Design of steel structures - Part 1-1: General rules for buildings; 2015.
[54] Beg D, Kuhlmann U, Davaine L, Braun B. Design of plated structures: eurocode 3: design of steel structures, part 1–5: design of plated structures. ECCS-European Convention for Constructional Steelwork 2012. https://doi.org/10.1002/9783433601143.fmatter.
[55] Statens-Vegvesen. The Hardanger Bridge: Design basis - Wind characteristics. Norway; 2006.
[56] Winterstein SR. Environmental contours : including the effects of directionality and other sub- probability-based engineering; 2018. https://doi.org/10.13140/RG.2.2.27196.69763.
[57] Haghayeghi ZS, Ketabdari MJ. A long-term joint probability model for metocean circular and linear characteristics. Appl Ocean Res 2018;75:143–52. https://doi.org/10.1016/j.apor.2018.03.009.
[58] Vanem E, Hafver A, Nalvarte G. Environmental contours for circular-linear variables based on the direct sampling method. Wind Energy 2020;23:563–74. https://doi.org/10.1002/we.2442.
[59] Fenerci A, Øiseth O, Rönnquist A. Long-term monitoring of wind field characteristics and dynamic response of a long-span suspension bridge in complex terrain. Eng Struct 2017;147:269–84. https://doi.org/10.1016/j.engstruct.2017.05.070.
[60] Fenerci A, Kvåle KA, Wiig Petersen Ø, Rønnquist A, Øiseth O. Wind and acceleration data from the Hardanger Bridge. Nor Univ Sci Technol 2020. https://doi.org/10.21400/5ng8980s.
[61] Fenerci A, Kvåle KA, Wiig Petersen Ø, Rønnquist A, Øiseth O. Dataset from long-term wind and acceleration monitoring of the Hardanger Bridge. J Struct Eng 2021;Forthcomin. https://doi.org/10.1061/(ASCE)ST.1943-541X.0002997.